ACS APPLIED MATERIALS & INTERFACES

Research Article

www.acsami.org

Smoothly Tunable Surface Properties of Aluminum Oxide Core–Shell Nanoparticles By A Mixed-Ligand Approach

Luis Portilla and Marcus Halik*

Organic Materials & Devices (OMD), Institute of Polymer Materials, University Erlangen-Nürnberg, Martensstraße 7, 91058 Erlangen, Germany

Supporting Information

ABSTRACT: We present a facile solution-based procedure for tailoring the surface properties of aluminum oxide nanoparticles (AlO_x-NPs) by the formation of tunable core–shell systems with self-assembled monolayers. By employing chained molecules with a phosphonic acid anchor group and either hydrophobic or hydrophilic chains the surface properties of the nanoparticles change dramatically. So, the solubility can be tuned orthogonal from trifluorotoluene (CF_3–C_6H_5) for hydrophobic shell to water (H_2O) for hydrophilic functionalization respectively. Spray coated films of those functionalized nanoparticles exhibited superhydrophobic or superhydrophilic properties. The surface properties can be tuned smoothly by the formation of a mixed ligand monolayer from corresponding stoichiometric mixtures of the ligands. The core–shell nanoparticles were investigated by means of thermogravimetric analysis, TGA; Fourier transform infrared spectroscopy, FTIR; and static contact angle goniometry, SCA. The effect of different dipole moments of the SAM molecules in mixed shell nanoparticles to their stability in dispersions was studied by zeta potential measurements.

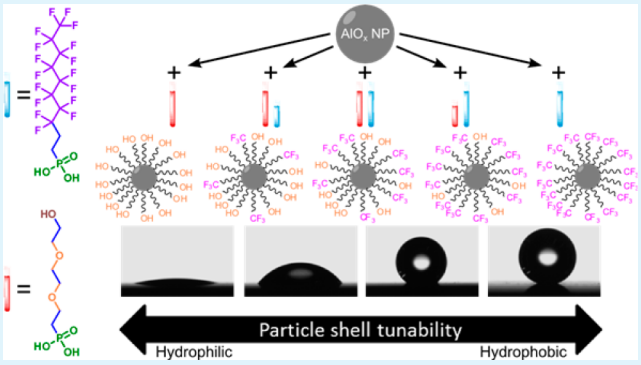

KEYWORDS: *nanoparticles, functionalization, aluminum oxide, hydrophobic, hydrophilic*

INTRODUCTION

Interactions between materials, surfaces, and solvents are mostly governed by their surface properties. The modification of a surface at nanoscale by introducing an organic molecular monolayer can dramatically change the overall behavior of the material both at the bulk and nano level. Nonetheless, while still being able to maintain most, if not all of the underlying material original properties. By this approach fundamentally, a myriad of new building blocks of matter can be engineered. Applications of self-assembled monolayers (SAMs) as surface control agents have been implemented in organic thin-film transistors (OTFTs),[1,2] dye-synthesized solar cells (DSSCs),[1] biosensors,[1] corrosion inhibition,[1] nanoparticle solubility,[3−5] antifogging-self-cleaning materials,[6] as well as directed self-assembly of nanoparticles,[7] among many others.[1]

In this work, we present a simple and versatile solution process for the surface functionalization of oxide nanoparticles. We have chosen AlO_x-NPs as model core system with an average diameter of 50 nm. The formation of core–shell NPs is carried out by molecular self-assembly of long chained alkyl phosphonic acids (PAs) until surface saturation. Variations in chain composition enable the control of solubility (even in orthogonal solvents), thin-film properties or NP stability in dispersions.

To investigate the SAM formation reaction and to optimize the full surface coverage of SAMs on AlO_x-NPs, we used simple hexadecylphosphonic acid [C_{16}–PA **1**]. Once the optimal functionalization parameters had been determined, particles were functionalized with PA molecules with either a hydrophobic or hydrophilic chain. Hydrophobicity is served by the partially fluorinated alkyl chain of 3,3,4,4,5,5,6,6,7,7,8,8,9,9,10,10,10-heptadecafluorodecylphosphonic acid [$F_{17}C_{10}$-PA **2**] and hydrophilic properties relay on the oligo glycol structure terminated with a hydroxyl group of (2-{2-[2-Hydroxy-ethoxy]-ethoxy}-ethyl)phosphonic acid [H-$(OC_2H_4)_3$-PA **3**]. Additionally, particles were modified with mixed monolayers of both molecules **2** and **3** in several stoichiometric ratios. Stoichiometric mixtures of self-assembled monolayers on flat AlO_x surfaces have been previously confirmed.[8,9]

The wettability characteristics were measured by formation of a nanoparticle film. Typically, in order to achieve the fabrication of superhydrophobic or superhydrophilic surfaces, a rough surface is a prerequirement. Surface roughness will amplify both of these effects correspondingly, making the hydrophilic surface more hydrophilic and the hydrophobic more hydrophobic.[6,10−13] However, in this case, fabrication of a superhydrophobic or superhydrophilic surface is achieved in a

Received: February 25, 2014
Accepted: March 25, 2014
Published: March 25, 2014

   dx.doi.org/10.1021/am501155r | ACS Appl. Mater. Interfaces 2014, 6, 5977−5982

single step by simply spray coating the nanoparticles on a flat surface. Because the nanoparticle surface properties have been previously modified, no additional processing is required after application of the nanoparticles, except for the removal of the carrier solvent. Furthermore, the broad particle size distribution and the poor deposition controllability obtained by spray coating leads to the formation of a rough nanoparticle film which further dramatizes the wettability properties. These factors allow the nanoparticle dispersion to be applied virtually to any surface in a paintlike manner. Moreover, the wettability of the films can be meticulously tuned from superhydrophobic to superhydrophilic by grafting mixed monolayers onto the nanoparticles surfaces.

As expected, it was observed that the nanoparticle dispersions exhibit decreased tendency to agglomerate with increased degree of functionalization of the nanoparticles surface. Stable dispersions (several hundred hours) of non-agglomerated NPs are obtained in hydrophobic solvent $CF_3-C_6H_5$ for $F_{17}C_{10}$-PA-terminated NPs and in H_2O for $H(OC_2H_4)_3$-PA-terminated NPs, respectively. However, the particles modified with mixed monolayers exhibited poor dispersibility at certain stoichiometric ratio. It is well-known that an electrostatic potential can be created by tightly packed (2D) organic monolayers. In addition, the magnitude of such potential is governed by the nature of the dipole moment of the molecules forming the layer.[14−17] Such an effect can be witnessed at the nanoparticle surface as evidenced by zeta potential measurements, and it is responsible for the stability of the nanoparticle dispersions in conjunction with the nanoparticle surface chemical nature.

EXPERIMENTAL DETAILS

Aluminum Oxide Nanoparticles. The aluminum oxide nanoparticles employed were purchased from Sigma Aldrich (part #: 702129). The particles were originally dispersed in 2-propanol with a concentration of 20 wt % and had an average size of 50 nm. Manufacturer did not specify the use of any dispersant. Prior to the processing of the nanoparticles, the particles were diluted to a concentration of 0.2 wt % by adding the required amount of 2-propanol, followed by an ultrasonic bath (15 min.) for proper redispersion.

Dynamic Light Scattering. Nanoparticle size distribution was obtained by measuring a 0.2 wt % dispersion of nanoparticles in 2-Propanol (Zetasizer Nano, Malvern, U. K.). Before measurement, particles were passed through a 0.8 μm PTFE membrane filter.

Functionalization with Hexadecylphosphonic Acid [C_{16}−PA 1]. The C_{16}−PA functionalizer solutions were prepared by dissolving C_{16}−PA into 2-propanol in different concentrations of 2.5, 5, 10, 20, and 40 mM, respectively. The functionalization procedure took place by adding 3 mL of the C_{16}−PA solution to 10 mL of the 0.2 wt % nanoparticle solution for every concentration of the C_{16}−PA solutions mentioned. The mixed solution was then placed in an ultrasonic bath for 30 min. The particles were then centrifuged and redispersed (×3) in pure 2-propanol for washing in order to remove any excess of ligands. Finally, dried overnight in a dry air oven at 80 °C prior to characterization. The C_{16}−PA was purchased from Sigma Aldrich (U.S.A) and used as-received.

Functionalization with 3,3,4,4,5,5,6,6,7,7,8,8,9,9,10,10,10-Heptadecafluorodecylphosphonic Acid [$F_{17}C_{10}$-PA 2] and (2-{2-[2-Hydroxy-ethoxy]-ethoxy}-ethyl)phosphonic Acid [H-$(OC_2H_4)_3$-PA 3]. The functionalization procedure with $H(OC_2H_4)_3$-PA and/or $F_{17}C_{10}$-PA was the same as employed for C_{16}−PA. However, in this case the functionalizer solutions employed were prepared according to the following 0:1, 1:3, 1:1, 3:1 and 1:0 $F_{17}C_{10}$-PA:$H(OC_2H_4)_3$-PA ratios with an overall concentration of 10 mM. The $H(OC_2H_4)_3$-PA and $F_{17}C_{10}$-PA were purchased from SiKEMIA (France) and used as received.

Thermogravimetric Analysis (TGA). TGA of the nanoparticle dry powders were carried out under a N_2 atmosphere at a heating rate of 10 °C/min up to 700 °C (Q500, TA Instruments, U.S.A.).

Fourier Transform Infrared Spectroscopy (FT-IR). FT-IR ATR measurements of the nanoparticle dry powder were obtained (IR Prestige-21, Shimadzu, Japan) utilizing an ATR setup with a Diamond/ZnSe crystal plate (MIRacle ATR, Pike Technologies, U.S.A.). Transmission spectra were collected at a resolution of 8 cm^{-1} (64 scans) by clamping dry nanoparticle powder to the ATR crystal plate.

Spray Coating of Nanoparticle Films. Nanoparticle films were manually spray-coated onto Si/SiO_2 wafers with a 100 nm thermal oxide layer. Before deposition of the films, the wafers were cleaned with a 3 min oxygen plasma treatment at 200 W at a pressure of 0.2 mbar (Pico, Diener electronic GmbH, Germany). Substrate was heated up to 80 °C during the spray coating process. The spray coating process was performed until the formation of a film was optically evident. Film morphology and coverage was studied by AFM (see the Supporting Information, Figure 2)

Static Contact Angle (SCA). SCA measurements were investigated by the sessile drop method utilizing DI water, formamide and diiodomethane (1.0 μL) as probe liquids (Dataphysics OCA, Data Physics Instruments GmbH, Germany).

Zeta Potential. Nanoparticles dispersed in 2-Propanol (0.2 wt %) were placed inside a folded capillary cell (DTS1070, Malvern, U. K.) for carrying out zeta potential measurements (Zetasizer Nano, Malvern, U. K.). Zeta potential values were determined by measuring the electrophoretic mobility of the nanoparticles by employing laser Doppler anemometry technique.

RESULTS AND DISCUSSION

Functionalization with C_{16}−PA. To study the surface coverage of the phosphonic acid molecules on the particle surface, we employed the C_{16}−PA. During self-assembly onto the AlO_x-NP, the C_{16}−PA provides a hefty molecular weight that can be easily observed by TGA. Moreover, the FT-IR spectrum of C_{16}−PA consists of vibrations (C−H_2, C−H_3, C−

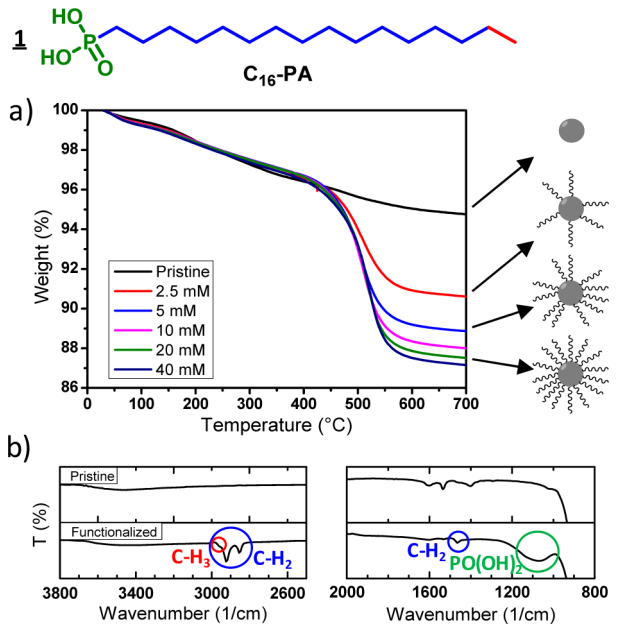

Figure 1. (a) TGA of AlO_x NPs functionalized with different concentrations of C_{16}−PA 1; (b) FTIR-ATR spectra of pristine and C_{16}−PA functionalized AlO_x NPs.

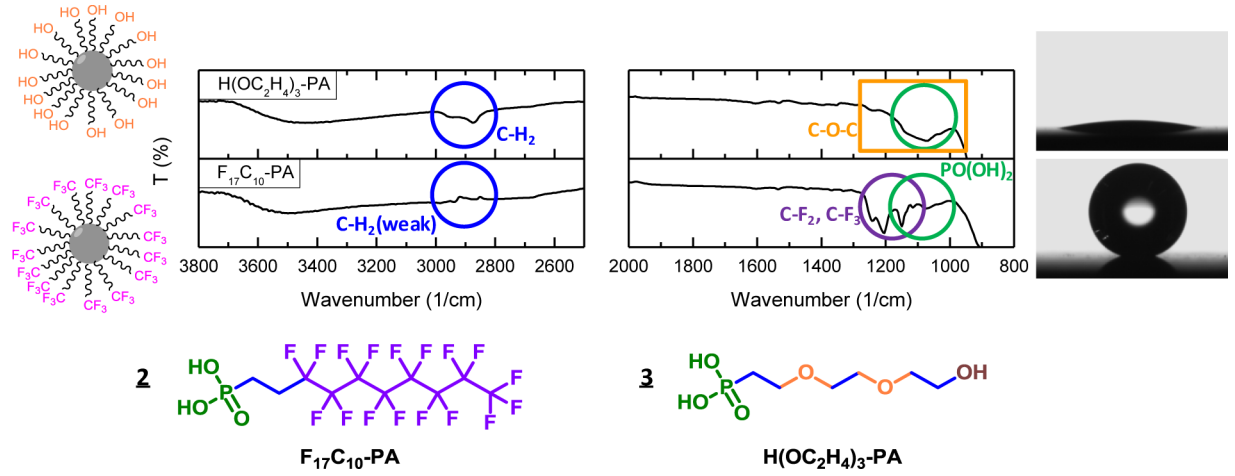

Figure 2. FTIR-ATR spectra of AlO_x NPs functionalized with $H(OC_2H_4)_3$-PA **3** and $F_{17}C_{10}$-PA **2**.

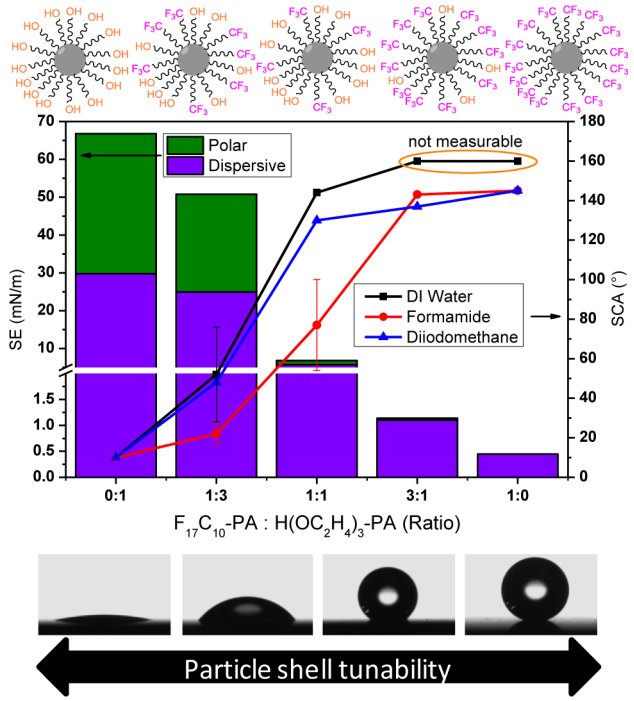

Figure 3. SCA measurements with different liquids and the calculated surface energy.

C, P−C, P−O, and P═O) that are easily detected by FT-IR spectroscopy.

The amount of C_{16}−PA molecules for complete functionalization of the nanoparticles was estimated using the DLS particle size distribution presented in the Supporting Information, Figure 1. Theoretical calculations were performed taking into account different grafting densities (4−7 molecules/nm^2) and assuming all particles being spherical for the calculation of the nanoparticle surface area (see the Supporting Information, Table 1). The particles were then functionalized employing different amounts of C_{16}−PA molecules (see the Supporting Information, Table 2). Even under the lowest concentration of C_{16}−PA employed (2.5 mM), the amount of ligand available for functionalization surpassed the theoretical amount needed for full coverage of the NPs. However, the TGA of the particles functionalized with different C_{16}−PA concentrations (Figure 1a) shows that chemisorpted C_{16}−PA to the nanoparticles reaches a maximum only around the 10 mM concentration. Therefore, the amount of ligand required for full coverage can be easily underestimated. In addition, when the overall mass loss is observed, it is evident that within the time frame of the functionalization step (30 min.) surface coverage can be slightly increased by employing the higher concentrations of 20 mM and 40 mM. A previous study on the kinetics of the self-assembly of similar molecules on flat alumina surfaces showed no significant change in packing density after exposure for 30 min.[18] It was therefore determined, that given the 30 min functionalization procedure, the ideal concentration for complete particle coverage of 10 mL of 0.2 wt % solution was 3 mL of 10 mM solution or higher. The thermal stability of the C_{16}−PA grafted ligands is observed to slightly exceed temperatures up to 400 °C, as no significant mass loss is observed below 400 °C. However, at higher temperatures the degradation of the organic layer becomes apparent due to the greater mass loss. Such mass loss is mainly attributed to the decomposition of the aliphatic carbon chains. The grafting density of the C_{16}−PA molecules to the particle surface was calculated accounting only for the mass drop % within the 400−600 °C region. It is between this temperature region that most of the mass loss occurs, as well as it is mostly due exclusively to the reduction of the organic layer engulfing the nanoparticles. The resulting grafting densities were estimated as 3.9, 5.3, 5.8, and 6.1 and 6.3 molecules per nm^2 for the 2.5, 5, 10, 20, and 40 mM concentrations respectively. Previous studies have suggested a grafting density of 4.6 molecules per nm^2 of octadecylphosphonic acid for fully covered flat alumina surfaces.[19] Therefore, for a nanoparticle surface, the maximum grafting density of approximately 6 molecules per nm^2 is in good agreement.

FTIR-ATR spectra of the dry functionalized nanoparticle powder exhibits clear evidence regarding the presence of the C_{16}−PA molecule. Figure 1b shows the obtained FTIR spectra for the pristine nanoparticle powder and the functionalized powder. The spectrum of the pristine nanoparticle powder shows an almost featureless progression plunging at 950 cm^{-1}, with the exception of three peaks of unidentified origin in the 1400−1600 cm^{-1} region. The source of such signals may be due to a stabilizing agent, impurities present, or remaining solvent in the pristine nanoparticles. In contrast, the functionalized powders exhibit a broad signal from 1000 to 1200 cm^{-1} that is attributed to the overlap of the P−O and P═O

dx.doi.org/10.1021/am501155r | ACS Appl. Mater. Interfaces 2014, 6, 5977−5982

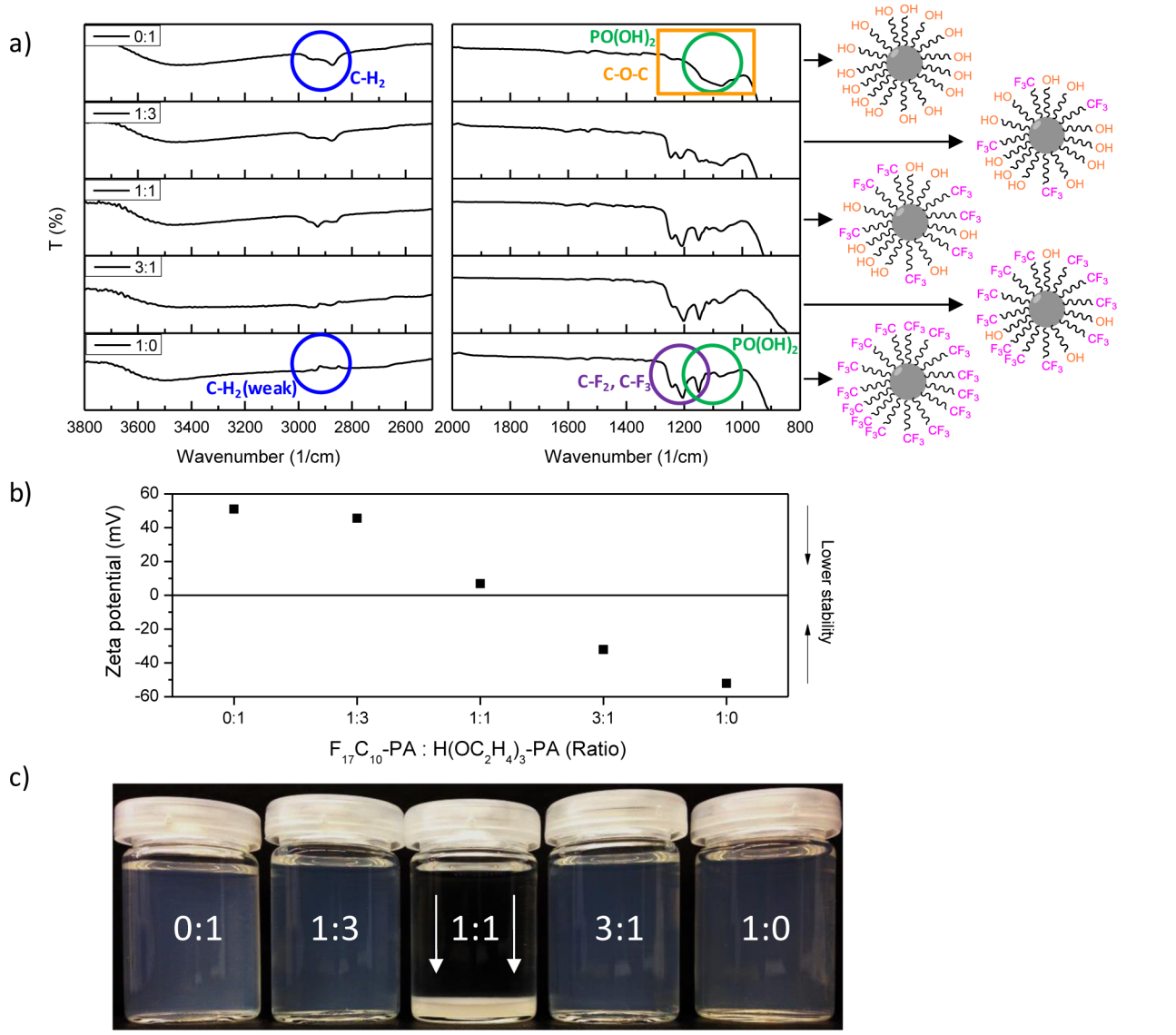

Figure 4. (a) FTIR-ATR spectra of particles functionalized with different ratios of $F_{17}C_{10}$-PA and $H(OC_2H_4)_3$-PA. (b) Zeta potential measurements of the nanoparticle dispersions in 2-propanol. (c) Image of the functionalized nanoparticle dispersions 20 min after redispersion by sonication.

vibrations of the phosphonic acid anchor groups bounded to the alumina surface.[20−22] The overlap comprises bounded or unbounded P−O and P═O groups signals, due to the likelihood of monodentate, bidentate, and tridentate binding modes coexisting on the particles surface.[23] The two peaks around 2850 and 2920 cm^{-1} correspond to the methylene groups vibrations of the C_{16}−PA aliphatic carbon chain, followed by a small shoulder appearing at 2970 cm^{-1} attributed to methyl groups at the tail of the alkyl chain. A less intense peak in the 1470 cm^{-1} region is recognized as methylene groups scissoring vibrations. Moreover, the peaks of unknown origin in the pristine powder are no longer present after functionalization.

Functionalization with a Mixed Monolayer. Formation of a mixed monolayer consisting of phosphonic acid molecules with a hydrophobic tail ($F_{17}C_{10}$-PA) and a hydrophilic tail ($H(OC_2H_4)_3$-PA) was grafted onto the alumina nanoparticles employing the previously described procedure. The concentration of each ligand in the functionalizer solution was varied proportionally in the rations of 0:1, 1:3, 1:1, 3:1, and 1:0, respectively, the overall concentration of both ligands was 10 mM.

The FTIR-ATR analysis of the nanoparticle dry powders is shown in Figure 2. The spectrum from the particles functionalized with $H(OC_2H_4)_3$-PA ligand (0:1) displays a broad valley from 1000 to 1200 cm^{-1} that corresponds to the P−O and P═O vibrations, comparable to the case of the C16-PA. However, in this case, the smoothness of the valley is compromised by the overlap of the C−O−C stretching vibrations which are present around the same region.[24] Similarly for the particles functionalized with $F_{17}C_{10}$-PA (1:0) an overlap between the bound phosphonic acid vibrations and the $C-F_2$ and $C-F_3$ occurs. The carbon fluorine vibrations are represented by the strong peaks at 1150 and 1200 cm^{-1} and by the smaller adjacent peak at 1250 cm^{-1}.[25,26]

Using functionalized nanoparticle dispersions in 2-propanol, nanoparticle films were spray coated onto a Si/SiO_2 wafer for static contact angle measurements and surface energy calculations (Figure 3). The film morphology was measured by AFM (see the Supporting Information, Figure 2), and the surface roughness of a 10 × 10 μm area was measured to be

approximately 100 nm RMS, which correlates agreeably to the particle size distribution measured. Spray-coated films of the 1:0 and 3:1 particles exhibited superhydrophobic properties with presumably DI water contact angles higher than 160°. The DI water contact angle of such films cannot be measured properly since the adhesion of the water droplet to the dispensing needle is higher than to the film (see the Supporting Information, Figure 3). As expected, the nanoparticle film hydrophobicity decreases for the films with a lesser degree of $F_{17}C_{10}$-PA in respect to the $H(OC_2H_4)_3$-PA, and vice versa in terms of hydrophilicity of the films. However, superhydrophilic properties only manifested in the nanoparticle film in which $F_{17}C_{10}$-PA was completely absent. The same tendency in wetting was observed when the films were probed using diiodomethane and formamide. Using the contact angle measurements of the probing liquids, the surface energy of the films (not the nanoparticle surface) was calculated. Films consisting of particles functionalized only with $F_{17}C_{10}$-PA presented an extremely low total surface energy of 0.45 mN/m, whereas films with $H(OC_2H_4)_3$-PA NPs exhibited a much higher surface energy of 67 mN/m.

Further evidence of the presence of a mixed monolayer is shown in FTIR spectra of particles functionalized with the 1:3, 1:1 and 3:1 ratios (Figure 4a). In particular for the 1:3 spectrum a clear superposition of the 1:0 and 0:1 signals can be observed. Equally, for all the spectra the two small peaks at 2850 and 2920 cm^{-1} relate to the $C-H_2$ group vibrations. Finally, a trend in intensity is also observable for the methylene groups when comparing the signals of the $H(OC_2H_4)_3$-PA (0:1) which possesses six methylene groups against the $F_{17}C_{10}$-PA (1:0) with only two methylene groups. Our investigation method on those mixed NPs does not allow us to make conclusions on the local morphology of the SAMs on the NP surface (e.g., formation of random, striped or Janus-type SAM structure),[27] but from previous work we expect, that the formation of mixed PA-based SAMs on AlO_x occurs randomly under these conditions.[28−30]

Zeta Potential. Nanoparticles functionalized with H-(OC2H4)3-PA exhibited a positive zeta potential of approximately +50 mV (Figure 4b). Having such a high zeta potential renders the nanoparticles highly dispersible in solution.[5] Likewise, particles functionalized with $F_{17}C_{10}$-PA show a negative zeta potential of −50 mV making them equally dispersible. However, when a 1:1 mixed ligand monolayer is grafted onto the nanoparticles the measured zeta potential is nearly zero, which in turn causes the dispersibility of the particles to be very poor (Figure 4c). Such an effect is attributed to the formation of a randomly ordered mixed monolayer of both ligands, effectively canceling out the electrostatic potential induced by either ligand. Under such conditions, agglomeration of the particles will occur because of the increased number of particle-to-particle interactions.

CONCLUSION

A versatile and simple wet-chemical approach for functionalization of alumina nanoparticles with phosphonic acid molecules is demonstrated. Moreover, the method allows for the coverage of the nanoparticle surface with a mixed monolayer only by proportionally varying the phosphonic acid ligands concentrations. The nanoparticle surface was successfully modified to exhibit hydrophobic or hydrophilic properties by employing different ligands. Superhydrophobic or superhydrophilic films were fabricated by providing both the desired surface energy and high surface roughness required in a single step process via spray coating. Furthermore, the wettability of the films can be tuned to any value by employing the mixed monolayer approach. The dispersibility of the particles in solution was demonstrated to be governed by the zeta potential of the particles. In turn, the magnitude of the zeta potential was greatly affected by the nature of the ligands grafted onto the nanoparticle. Such effects are of concern regarding the further processability of the nanoparticle dispersion in terms of agglomeration and sedimentation. Lastly, because of the affinity of phosphonic acids to a variety of other metal oxides,[2] the validity of this method could be in principle extended to other materials, thus allowing not only for surface modification of AlO_x-NPs but also for innumerable core−shell configurations.

ASSOCIATED CONTENT

Supporting Information

Supplementary details on particle size distribution, SAM grafting densities, AFM images, and two links to movies illustrating the surface wetting behavior. This material is available free of charge via the Internet at http://pubs.acs.org.

AUTHOR INFORMATION

Corresponding Author

*E-mail: marcus.halik@fau.de.

Notes

The authors declare no competing financial interest.

ACKNOWLEDGMENTS

The authors are grateful for financial support by the Graduate School 1161 "Disperse Systems for Electronic Applications" funded by DFG and Evonik Degussa GmbH, Germany as well as for additional support by the Cluster of Excellence "Engineering of Advanced Materials" funded by Deutsche Forschungsgemeinschaft (DFG).

REFERENCES

(1) Guerrero, G.; Alauzun, J. G.; Granier, M.; Laurencin, D.; Mutin, P. H. Phosphonate Coupling Molecules for the Control of Surface/Interface Properties and the Synthesis of Nanomaterials. *Dalton Trans.* **2013**, *42*, 12569−12585.

(2) Halik, M.; Hirsch, A. The Potential of Molecular Self-Assembled Monolayers in Organic Electronic Devices. *Adv. Mater.* **2011**, *23*, 2689−2695.

(3) Crouse, C. A.; Pierce, C. J.; Spowart, J. E. Influencing Solvent Miscibility and Aqueous Stability of Aluminum Nanoparticles Through Surface Functionalization with Acrylic Monomers. *ACS Appl. Mater. Interfaces* **2010**, *2*, 2560−2569.

(4) Faure, B.; Salazar-Alvarez, G.; Ahniyaz, A.; Villaluenga, I.; Berriozabal, G.; De Miguel, Y. R.; Bergström, L. Dispersion and Surface Functionalization of Oxide Nanoparticles for Transparent Photocatalytic and UV-Protecting Coatings and Sunscreens. *Sci. Technol. Adv. Mater.* **2013**, *14*, 023001.

(5) Jiang, J.; Oberdörster, G.; Biswas, P. *J.* Characterization of Size, Surface Charge, and Agglomeration State of Nanoparticle Dispersions for Toxicological Studies. *Nanoparticle Res.* **2008**, *11*, 77−89.

(6) Feng, L.; Li, S.; Li, Y.; Li, H.; Zhang, L.; Zhai, J.; Song, Y.; Liu, B.; Jiang, L.; Zhu, D. Super-Hydrophobic Surfaces: From Natural to Artificial. *Adv. Mater.* **2002**, *14*, 1857−1860.

(7) Grzelczak, M.; Vermant, J.; Furst, E. M.; Liz-Marzán, L. M. Directed Self-Assembly of Nanoparticles. *ACS Nano* **2010**, *4*, 3591−3605.

(8) Zschieschang, U.; Ante, F.; Schlörholz, M.; Schmidt, M.; Kern, K.; Klauk, H. Mixed Self-Assembled Monolayer Gate Dielectrics for

Continuous Threshold Voltage Control in Organic Transistors and Circuits. *Adv. Mater.* **2010**, *22*, 4489−4493.
(9) Jedaa, A.; Salinas, M.; Jäger, C. M.; Clark, T.; Ebel, A.; Hirsch, A.; Halik, M. Mixed Self-Assembled Monolayer of Molecules with Dipolar and Acceptor Character—Influence on Hysteresis and Threshold Voltage in Organic Thin-Film Transistors. *Appl. Phys. Lett.* **2012**, *100*, 063302.
(10) Lafuma, A.; Quéré, D. Superhydrophobic States. *Nat. Mater.* **2003**, *2*, 457−460.
(11) Quéré, D. Rough Ideas on Wetting. *Phys. A* **2002**, *313*, 32−46.
(12) Nakajima, A.; Fujishima, A.; Hashimoto, K.; Watanabe, T. Preparation of Transparent Superhydrophobic Boehmite and Silica Films by Sublimation of Aluminum Acetylacetonate. *Adv. Mater.* **1999**, *11*, 1365−1368.
(13) Darmanin, T.; Guittard, F.; Amigoni, S.; Tafin de Givenchy, E.; Noblin, X.; Kofman, R.; Celestini, F. Superoleophobic Behavior of Fluorinated Conductive Polymer Films Combining Electropolymerization and Lithography. *Soft Matter* **2011**, *7*, 1053.
(14) Cahen, D.; Naaman, R.; Vager, Z. The Cooperative Molecular Field Effect. *Adv. Funct. Mater.* **2005**, *15*, 1571−1578.
(15) Salinas, M.; Jäger, C. M.; Amin, A. Y.; Dral, P. O.; Meyer-Friedrichsen, T.; Hirsch, A.; Clark, T.; Halik, M. The Relationship Between Threshold Voltage and Dipolar Character of Self-Assembled Monolayers in Organic Thin-Film Transistors. *J. Am. Chem. Soc.* **2012**, *134*, 12648−12652.
(16) Kobayashi, S.; Nishikawa, T.; Takenobu, T.; Mori, S.; Shimoda, T.; Mitani, T.; Shimotani, H.; Yoshimoto, N.; Ogawa, S.; Iwasa, Y. Control of Carrier Density by Self-Assembled Monolayers in Organic Field-Effect Transistors. *Nat. Mater.* **2004**, *3*, 317−322.
(17) Chung, Y.; Verploegen, E.; Vailionis, A.; Sun, Y.; Nishi, Y.; Murmann, B.; Bao, Z. Controlling Electric Dipoles in Nanodielectrics and its Applications for Enabling Air-Stable n-Channel Organic Transistors. *Nano Lett.* **2011**, *11*, 1161−1165.
(18) Lenz, T.; Schmaltz, T.; Novak, M.; Halik, M. Self-Assembled Monolayer Exchange Reactions as a Tool for Channel Interface Engineering in Low-Voltage Organic Thin-Film Transistors. *Langmuir* **2012**, *28*, 13900−13904.
(19) Klauk, H.; Zschieschang, U.; Pflaum, J.; Halik, M. Ultralow-Power Organic Complementary Circuits. *Nature* **2007**, *445*, 745−748.
(20) Pawsey, S.; Yach, K.; Reven, L. Self-Assembly of Carboxyalkylphosphonic Acids on Metal Oxide Powders. *Langmuir* **2002**, *18*, 5205−5212.
(21) Zenobi, M. C.; Luengo, C. V; Avena, M. J.; Rueda, E. H. An ATR-FTIR Study of Different Phosphonic Acids Adsorbed onto Boehmite. *Spectrochim. Acta, Part A* **2010**, *75*, 1283−1288.
(22) Cinausero, N.; Azema, N.; Cochez, M.; Ferriol, M.; Essahli, M.; Ganachaud, F.; Lopez-Cuesta, J.-M. Influence of the Surface Modification of Alumina Nanoparticles on the Thermal Stability and Fire Reaction of PMMA Composites. *Polym. Adv. Technol.* **2008**, *19*, 701−709.
(23) Bauer, T.; Schmaltz, T.; Lenz, T.; Halik, M.; Meyer, B.; Clark, T. Phosphonate- and Carboxylate-Based Self-Assembled Monolayers for Organic Devices: A Theoretical Study of Surface Binding on Aluminum Oxide with Experimental Support. *ACS Appl. Mater. Interfaces* **2013**, *5*, 6073−6080.
(24) Charpentier, P. A.; Burgess, K.; Wang, L.; Chowdhury, R. R.; Lotus, A. F.; Moula, G. Nano-TiO2/Polyurethane Composites for Antibacterial and Self-Cleaning Coatings. *Nanotechnology* **2012**, *23*, 425606.
(25) Paniagua, S. A.; Hotchkiss, P. J.; Jones, S. C.; Marder, S. R.; Mudalige, A.; Marrikar, F. S.; Pemberton, J. E.; Armstrong, N. R. Phosphonic Acid Modification of Indium−Tin Oxide Electrodes: Combined XPS/UPS/Contact Angle Studies. *J. Phys. Chem. C* **2008**, *112*, 7809−7817.
(26) Gao, X.; Chorover, J. Adsorption of Perfluorooctanoic Acid and Perfluorooctanesulfonic Acid to Iron Oxide Surfaces as Studied by Flow-Through ATR-FTIR Spectroscopy. *Environ. Chem.* **2012**, *9*, 148.
(27) Liu, X.; Yu, M.; Kim, H.; Mameli, M.; Stellacci, F. Determination of Monolayer-Protected Gold Nanoparticle Ligand−Shell Morphology Using NMR. *Nat. Commun.* **2012**, *3*, 1182.
(28) Burkhardt, M.; Jedaa, A.; Novak, M.; Ebel, A.; Voïtchovsky, K.; Stellacci, F.; Hirsch, A.; Halik, M. Concept of a Molecular Charge Storage Dielectric Layer for Organic Thin-Film Memory Transistors. *Adv. Mater.* **2010**, *22*, 2525−2528.
(29) Rumpel, A.; Novak, M.; Walter, J.; Braunschweig, B.; Halik, M.; Peukert, W. Tuning the Molecular Order of C_{60} Functionalized Phosphonic Acid Monolayers. *Langmuir* **2011**, *27*, 15016−15023.
(30) Jäger, C. M.; Schmaltz, T.; Novak, M.; Khassanov, A.; Vorobiev, A.; Hennemann, M.; Krause, A.; Dietrich, H.; Zahn, D.; Hirsch, A.; Halik, M.; Clark, T. Improving the Charge Transport in Self-Assembled Monolayer Field-Effect Transistors: From Theory to Devices. *J. Am. Chem. Soc.* **2013**, *135*, 4893−4900.